Rapid Trapping and Label-free Optical Characterization of Single Nanoscale Extracellular Vesicles and Nanoparticles in Solution

Ikjun Hong[1,2], Chuchuan Hong[1,2], Theodore Anyika[1,2], Guodong Zhu[1,2], and Maxwell Ugwu[1,3], James N. Higginbotham[4,7,8], Jeffrey L. Franklin[4,5,7,8], Robert Coffey[4,5,7,8], Justus C. Ndukaife[1,2,6,7]*
*Correspondence: justus.ndukaife@vanderbilt.edu

[1]Vanderbilt Institute of Nanoscale Science and Engineering, Vanderbilt University, Nashville, Tennessee, 37235, United States

[2]Department of Electrical and Computer Engineering, Vanderbilt University, Nashville, Tennessee, 37235, United States

[3]Interdisciplinary Materials Science and Engineering, Vanderbilt University, Nashville, Tennessee, 37235, United States

[4]Department of Medicine, Vanderbilt University Medical Center, Nashville, Tennessee 37232, United States

[5]Department of Cell and Developmental Biology, Vanderbilt University, Nashville, Tennessee 37232, United States

[6]Department of Mechanical Engineering, Vanderbilt University, Nashville, Tennessee 37235, United States

[7]Center for Extracellular Vesicles Research, Vanderbilt University, Nashville, Tennessee 37235, United States

[8]Epithelial Biology Center, Vanderbilt University Medical Center, Nashville, TN

S1. AC electro osmotic flow simulation

The AC electro-osmotic (ACEO) flows induced by the micron-scale hole array were simulated in COMSOL Multiphysics. First, the AC electric field distribution within the microfluidic chamber is calculated in a 3D computational domain by solving the Poisson equation given by:

$$\nabla \cdot \mathbf{E} = \frac{\rho}{\varepsilon_0}, \text{with } \mathbf{E} = -\nabla \mathrm{V}$$

, where $\mathbf{E}$ is the electric field, ρ is the local volume charge density, ε_0 is the permittivity, and V is the potential. The height of the microfluidic chamber is set to 120 μm, the thickness of the gold film is 15 nm, and the diameter of the micron-scale hole is 15 μm. Using the Electric Current module, the electric potential on the gold film side is set to 0 V, and on the ITO side to 3.53 V, which is corresponds to the root-mean-square value for an applied 10 V peak-to-peak voltage. A periodic boundary condition is applied along the side walls to mimic an infinite array of micron-scale holes, with 18 μm periodicity.

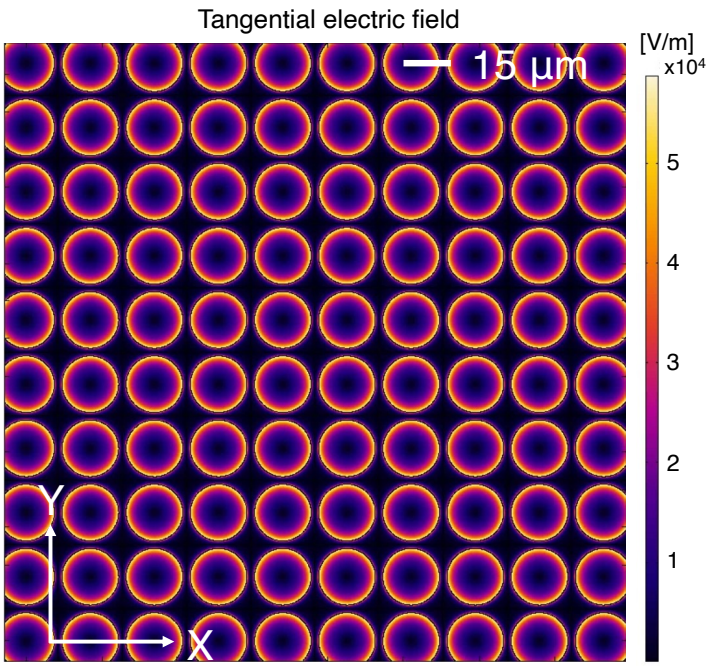

Supplementary Figure 1: The in-plane AC electric field distribution 500 nm above the surface.

Following the solution of the electric field distribution within the microfluidic channel, the Laminar Flow module is then used to calculate the flow velocity distribution for the induced AC electro-osmotic flow. To achieve this, we solved the Navier-Stokes equation in COMSOL Multiphysics given by:

$$\rho_0[\mathrm{u}(\mathbf{r})\cdot\nabla]\mathrm{u}(\mathbf{r}) + \nabla\rho(\mathbf{r}) - \eta\nabla^2\mathrm{u}(\mathbf{r}) = \mathbf{F}$$

, where ρ_0 is the density of the fluid, $\rho(\mathbf{r})$ is the pressure distribution, η is the viscosity of medium, $\mathrm{u}(\mathbf{r})$ is the fluid velocity, and $\mathbf{F}$ is the body force.

To account for the AC electroosmotic flow, we add a slip velocity boundary condition defined by the Helmholtz-Smoluchowski slip velocity with magnitude that is given by:

$$\boldsymbol{u}_s = -\frac{\varepsilon_w \zeta}{\eta}\mathbf{E}_{\parallel}$$

, where $\mathbf{u}_s$ is the velocity of the a.c. electro-osmotic flow, ε_w is the permittivity of the fluid medium, ζ is the zeta potential, η is the fluid viscosity, and $\mathbf{E}_{\parallel}$is the tangential component of the electric field established near the surface calculated by the electric current module. The zeta potential was set as -15 mV and the relative permittivity of the fluid was set as 78.

S2. Fabrication procedures

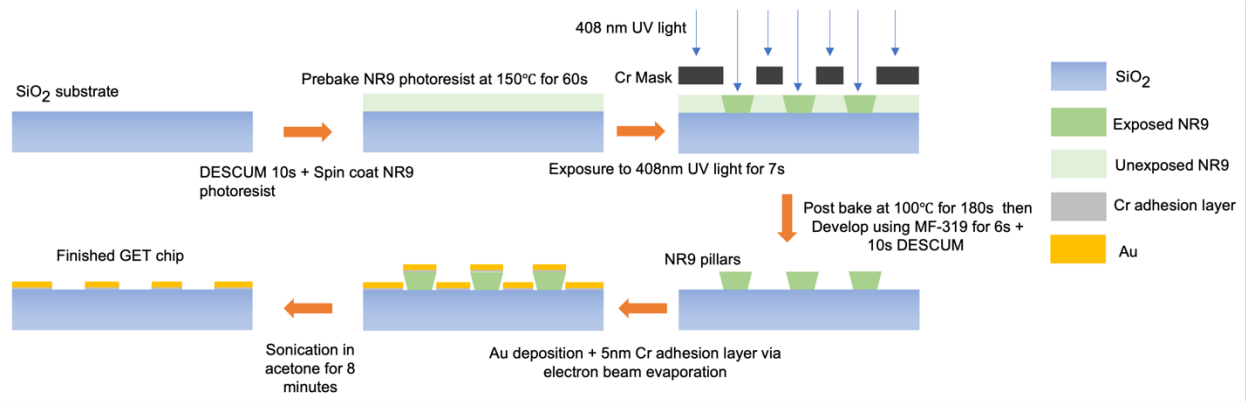

Supplementary Figure 2: The fabrication procedure outlines the individual steps for the large area fabrication of the nanotweezer device.

S3. SEM image

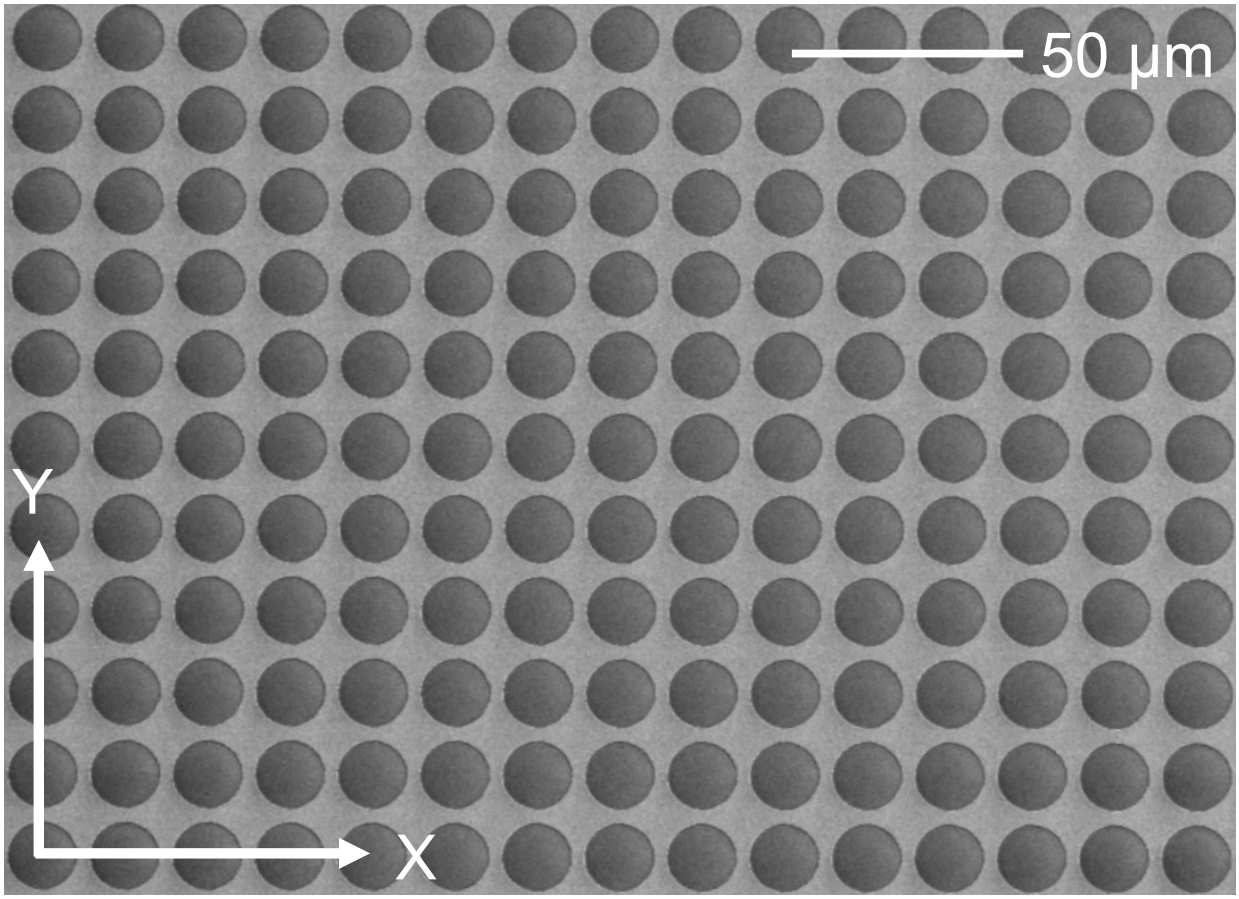

Supplementary Figure 3: The SEM image of the fabricated chip.

S4. MSD estimation of 100nm, 200 nm, and 300 nm PS particle.

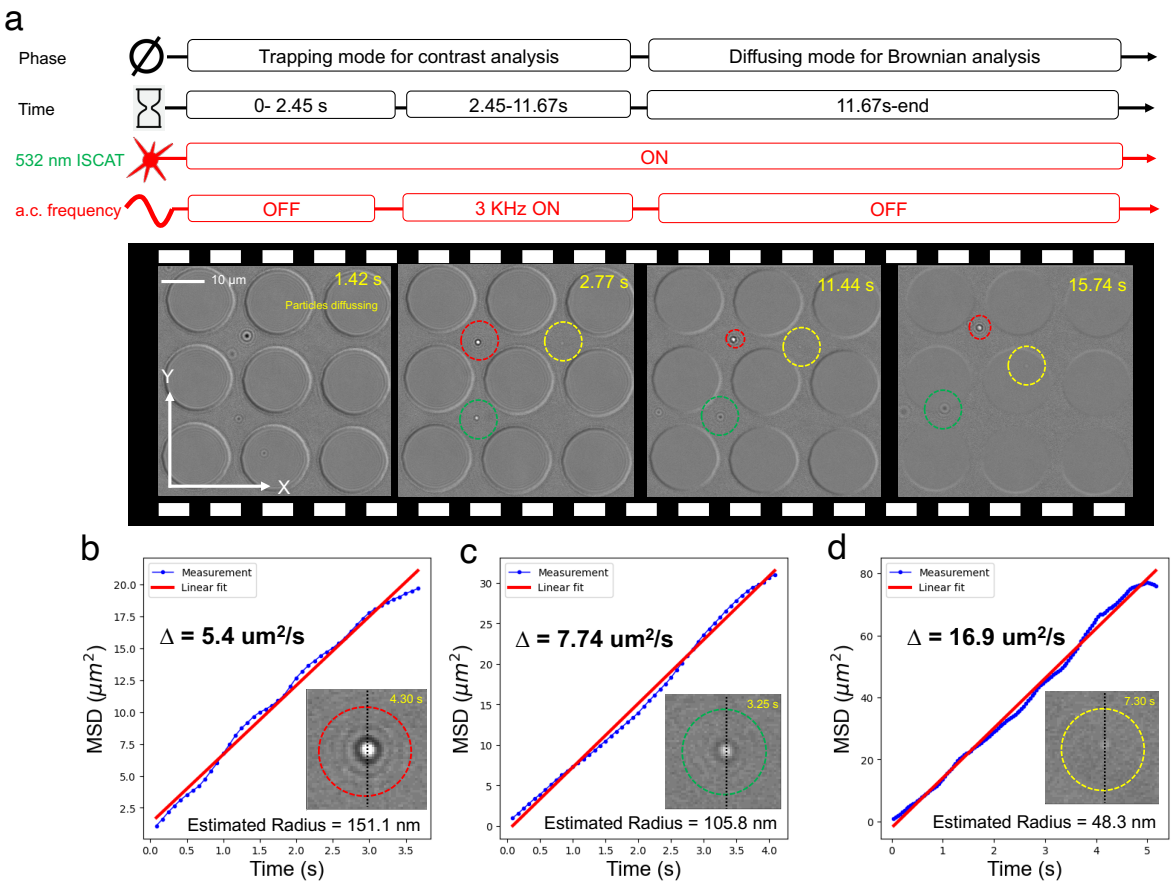

Supplementary Figure 4: Trapping and label-free detection of 100, 200, and 300 nm PS particles. a. Frame-by-frame images of the trapping experiment for 100, 200, and 300 nm PS particles under a 532 nm laser for ISCAT detection. b, c, d. MSD calculation with linear regression for the estimation of the diffusion coefficient for the three particles.

We trap and characterize the predefined size of particle from 100 nm, 200nm, and 300 nm polystyrene (PS) beads. Figure S4a describes the frame-by-frame events for both trapping and diffusing phases of experiment after the image processing. Trapping mode occurs when the AC field is on, and the particles are under trapped following ACEO flows. Diffusion mode happens when the AC field is off, and the particle undergoes

Brownian diffusion. Initially, the 100 nm, 200 nm, and 300 nm mixed particles in the DI water medium freely diffuse during the 0-2.45 s period, while the 532 nm ISCAT laser is prepared for imaging. The concentration of the mixed particles is $2x10^6$ particles/mL, and the field of view (FOV) is 50 μm x 50 μm for the ISCAT detection. When the 3 kHz AC field is turned on, the particles of different sizes become trapped during 2.45-11.67s period, marked by a red, yellow, and green dotted circle in Figure S4a. After trapping, the AC field is turned off to release the particles from the trapping site after 11.67 s. During diffusion mode, particles of different sizes undergo Brownian dynamics in the medium. Tracking the diffusion of particles in two dimensions with the mean-squared-displacement (MSD) of their trajectories provides the diffusion coefficients for each single particle, following the equation: $MSD(\tau) = \langle \Delta r(\tau)^2 \rangle = \langle [r(t+\tau) - r(t)]^2 \rangle$, where τ is the lag time, t is the designated time, and $r(t+\tau)$ is the position of particle at $t+\tau$ time frames. Each blue dotted line in Fig. S4b, c, and d represents the calculated MSD plot over the lag time.

The linear fitting slope of the MSD as marked by a red line provides the diffusion coefficient of each particle in the medium. During diffusion mode, particles of different sizes undergo Brownian dynamics in the medium, and the trajectory of each particle is depicted in Fig. 4b of the main manuscript. By tracking the diffusion of particles in two dimensions and calculating the mean-squared displacement (MSD) of their trajectories, we obtain the diffusion coefficients for each particle. The diffusion coefficient is calculated using the equation $D = \frac{MSD(\tau)}{4\tau} = \frac{\Delta}{4}$, where Δ is the slope of the linear fitting curve. The slopes (Δ) of regression line are 5.4 μm²/s, 7.91 μm²/s, and 16.9 μm²/s,

corresponding to estimated PS bead sizes of 151.1 nm, 103.6 nm, and 48.3 nm in radius, respectively.

S5. Trapping force for Raman analysis

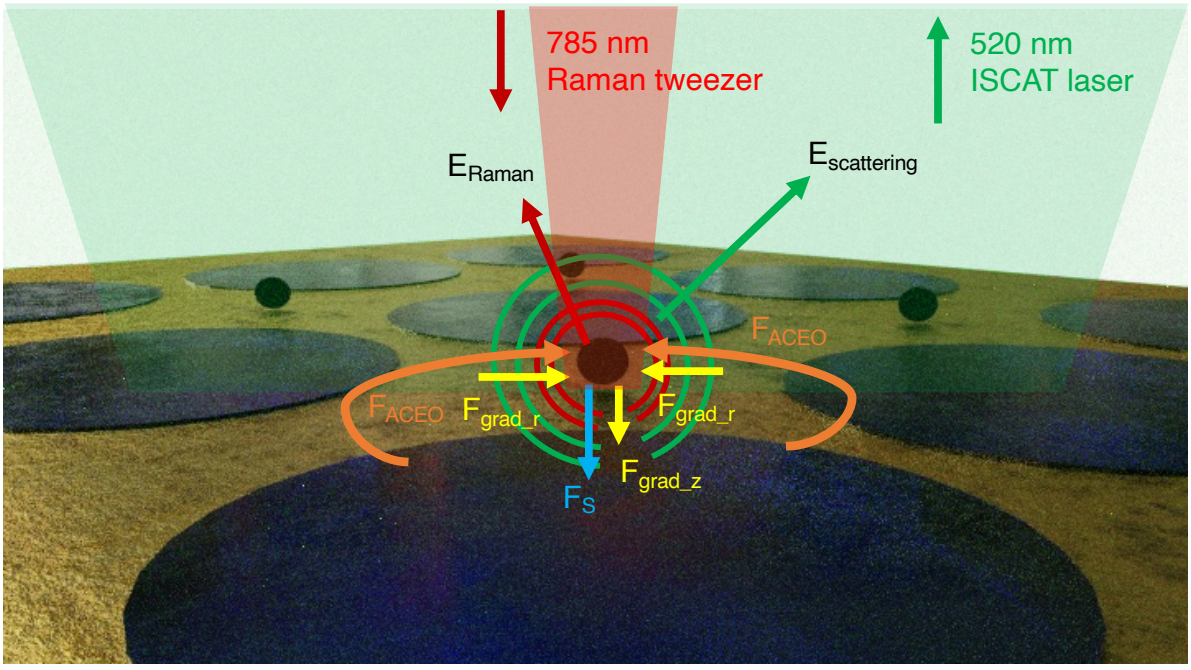

Supplementary Figure 5: The total force acting on the particle under the operation of Raman trapping with a label free detection.

For label-free detection, trapping, and Raman analysis, the 785 nm laser is focused through the water medium toward the gold film, while the 520 nm ISCAT laser passes through the thin gold film in transmission mode, as described in Figure 1b of the main text. Once the ACEO flow transports the particle to the stagnation zone, it is stably trapped. Next, the Raman excitation beam is focused on the particle to trap it more securely by the in-plane and out-of-plane optical gradient forces.

S6. Brownian motion of three different EVs.

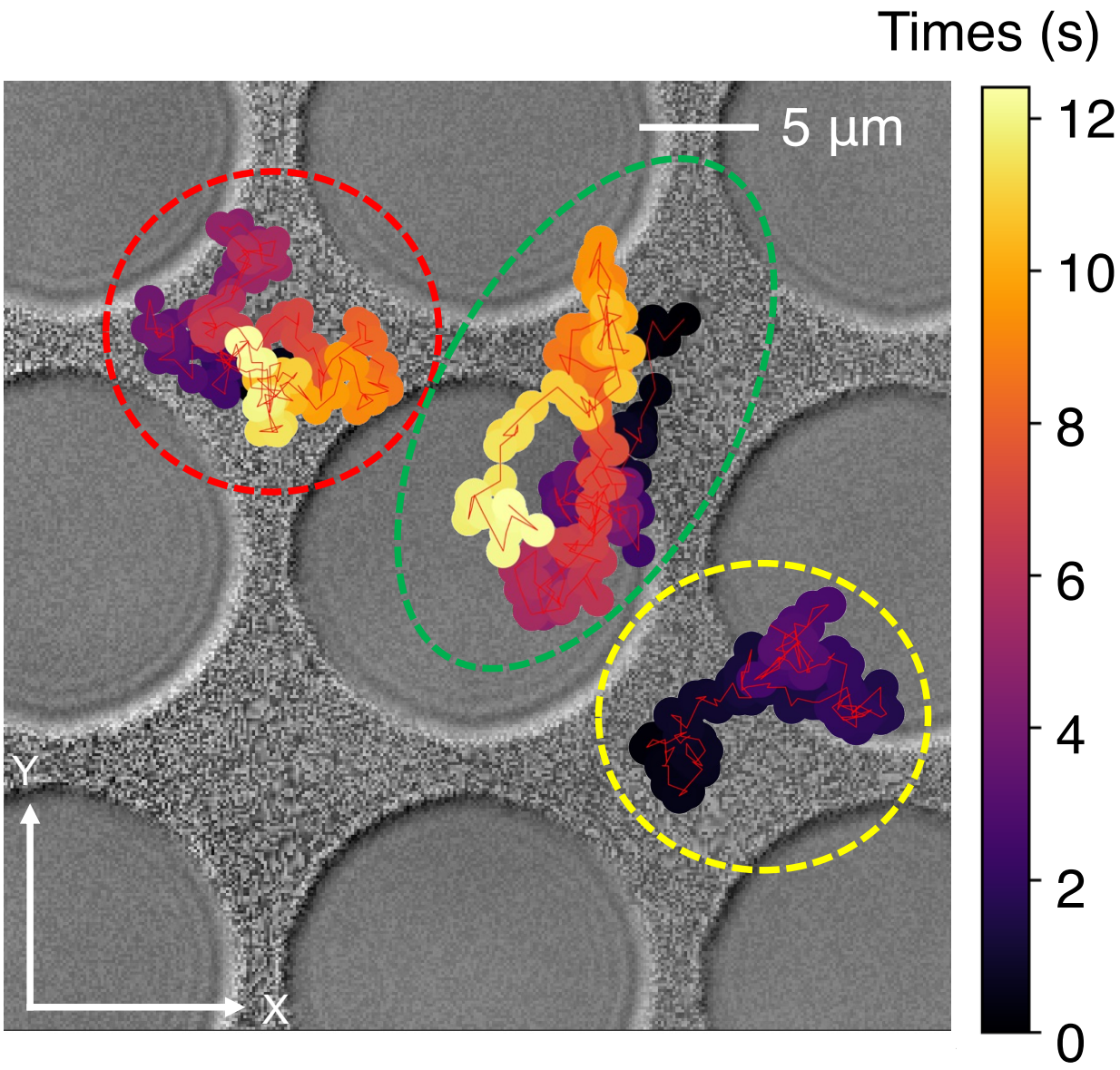

Supplementary Figure 6: Tracking the movement of EVs after release from the trapping site to quantify the diffusion coefficient of three different EVs.

To independently estimate the EV sizes and generate a calibration plot of their contrast images with respect to size, we released the EVs by temporarily turning OFF the applied AC field and tracking their Brownian dynamics. Figure S6 illustrates the

Brownian trajectories of three EVs, with the red, green, and yellow dotted lines tracing their movement in two-dimensional space. Particle localization is tracked over approximately 12 seconds, and the MSD for each EV is shown in Figure 5c, d, and e in the main text.

S7. Rotational motion of EV

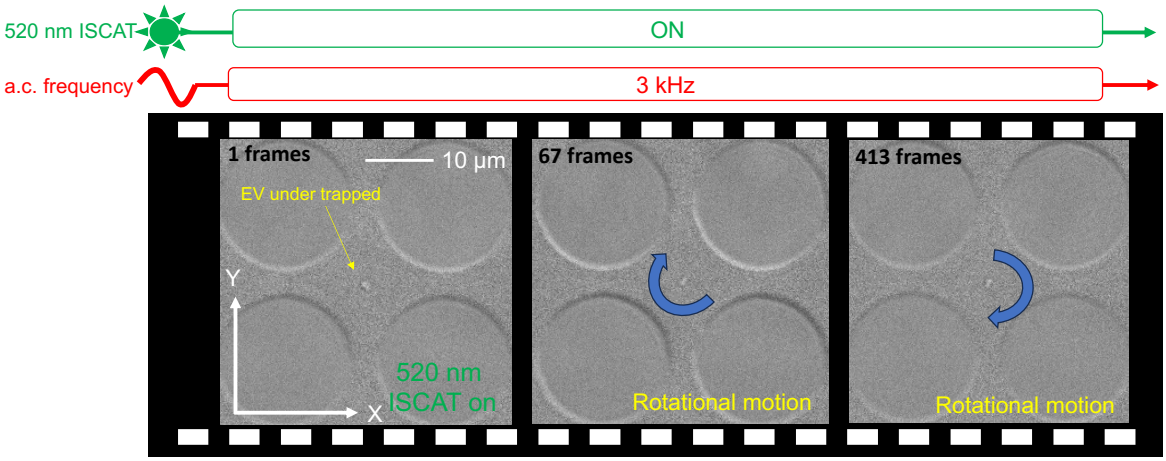

Supplementary Figure 7: The detection of rotational motion of an EV. The asymmetric shape of the EV induces a non-uniform force on the particle, leading to torque that causes the particle to rotate.

S8. Label-free trapping and detection of supermeres.

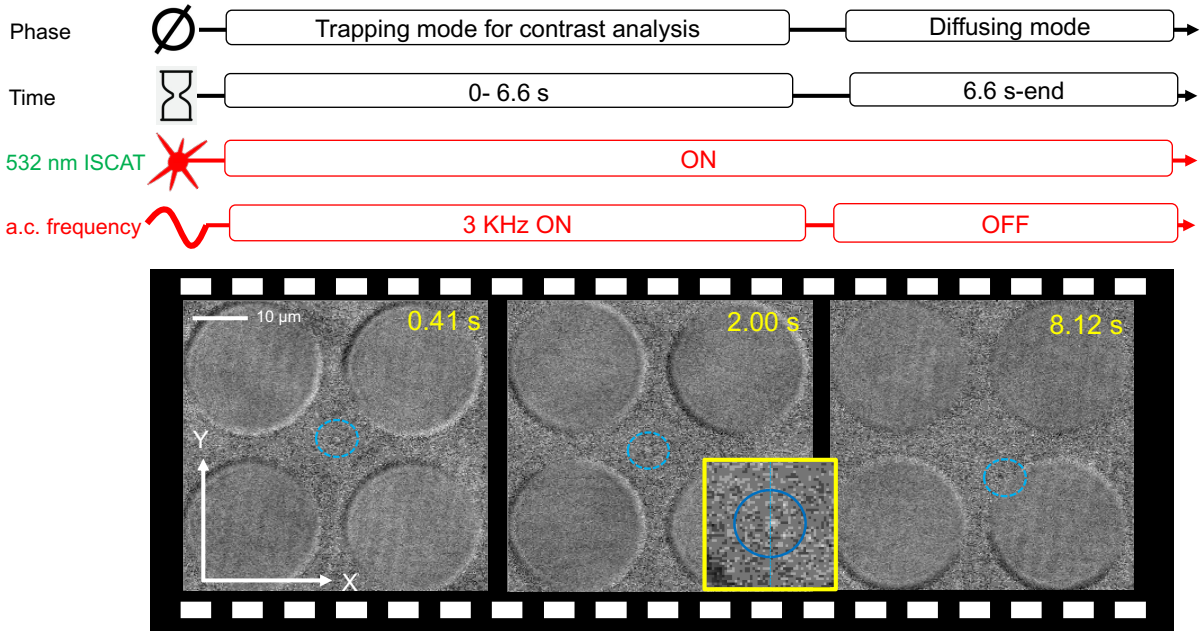

Supplementary Figure 8: Sequential images showing the trapping and release of supermeres.

S9. Raman analysis from large EV.

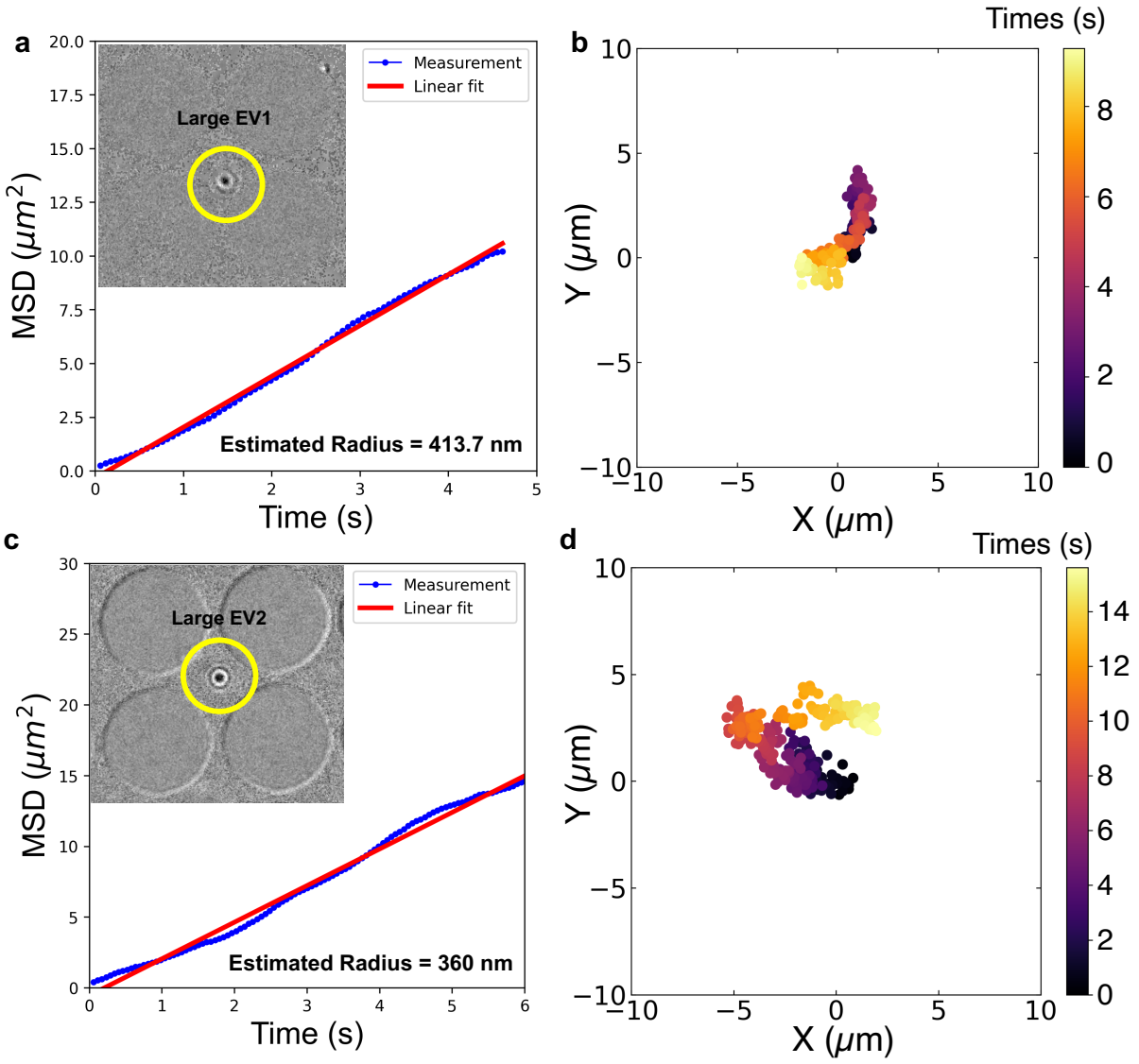

Supplementary Figure 9: The label-free detection and Raman analysis from a single large EV. (a, b) The size estimation of Large EV1 with a tracking motion of particle after releasing from the trapping site. (c, d) The size estimation of Large EV2 with a tracking motion of particle after releasing from the trapping site.

Raman measurements in Figures 5g and 5h are obtained from the large EVs 1 and 2, as shown in Figure S9. The Raman signal from a single EV in Figure 5g in the manuscript is collected from the particle depicted in the inset of Figure S9a. The MSD estimation suggests the particle has an estimated radius of approximately 413.7 nm and 360 nm, and the corresponding trajectory of this single EV is tracked and shown in Figure S9b. The Raman signal from a single EV in Figure 5h in the manuscript is collected from the particle depicted in the inset of Figure S9c, and its Brownian motion trajectory is shown in Figure S9d.

S10. EVs related Raman spectrum

Frequency (cm^{-1})	Biomolecule	Assignment
1550–1555	Proteins	Tryptophan (W3)
1515–1540	Carotenoids	Polyene v(C═C)
1450–1490	Nucleic acids	Purine adenine, guanine ring
1435–1465	Proteins	Backbone δ (CH_2, CH_3)
	Lipids	δ (CH_2, CH_3) in acyl chain
1300–1350	Proteins	Backbone δ ($C_\alpha H$), v(C_α–C)
1295–1305	Lipids	δ (CH_2) in acyl chain
1260–1270	Lipids	δ (═CH_2) in acyl chain
1230–1305	Proteins	Amide III: v (C–N) + δ (NH)
1207–1210	Proteins	Phenylalanine (F3), Tyrosine (Y3)
1175–1177	Proteins	Tyrosine (Y4)
1155–1160	Carotenoids	Polyene v(C–C)
1050–1160	Proteins	Backbone v(C_α–N, C_α–C, C–N)
1300–1350	Lipids	v(C–C) in acyl chain
1032	Proteins	Phenylalanine (F4)
1012	Proteins	Tryptophan (W6)
1004	Proteins	Phenylalanine (F5)

Frequency (cm^{-1})	Biomolecule	Assignment
930–960	Proteins	α-Helix backbone $\nu(C–C_\alpha–N)$
878–880	Proteins	Tryptophan (W7)
820–900	Phospholipids	$\nu(O–C–C–N^+)$, $\nu(C_4–N^+)$
810–836	Nucleic acids	Phosphodiester $\nu_s(O–P–O)$
758–759	Proteins	Tryptophan (W8)
725–751	Nucleic acids	Adenine
717	Phospholipids	$\nu_s(C–N^+)$
700–704	Lipids	Cholesterol

ν = Stretching mode, δ = deformation mode; This EV-related Raman table is quoted from Kruglik, Sergei G., et al. 'Raman tweezers microspectroscopy of circa 100 nm extracellular vesicles.[1]

S11. EV and supermere preparation.

EVs and supermeres were isolated from a hollow fiber bioreactor (FiberCell, New Market, MD) conditioned media from DiFi cells as described in [2], except that the second higher speed spin was at 2,500 x g not 1363 x g. Supermere and small EV pellets where purified as described in[3].

Movies:

Supplementary video 1: Rapid and parallel trapping of a 300 nm PS bead for the raw video.

Supplementary video 2: Rapid and parallel trapping of a 300 nm PS bead after the background subtraction.

Supplementary video 3: 100nm, 200 nm, and 300 nm PS beads trapping and releasing after the background subtraction.

Supplementary video 4: EVs trapping and release after the background subtraction.

Supplementary video 5: EVs rotational motion after the background subtraction showing that our approach can detect irregular shaped particles that are non-spherical such as two EVs fused together.

Supplementary video 6: Supermeres trapping and releasing after the background subtraction.

1. Kruglik, S. G. *et al.* Raman tweezers microspectroscopy of circa 100 nm extracellular vesicles. *Nanoscale* **11**, 1661–1679 (2019).
2. Hong, I. *et al.* Anapole-Assisted Low-Power Optical Trapping of Nanoscale Extracellular Vesicles and Particles. *Nano Lett* (2023).
3. Zhang, Q., Jeppesen, D. K., Higginbotham, J. N., Franklin, J. L. & Coffey, R. J. Comprehensive isolation of extracellular vesicles and nanoparticles. *Nat Protoc* **18**, 1462–1487 (2023).